MATEC Web of Conferences **33**, 05006 (2015)
DOI: 10.1051/matecconf/20153305006

Ab initio study of Ni_2MnGa under shear deformation

Martin Zelený[1,2,a], Ladislav Straka[3] and Alexei Sozinov[4]

[1]*Institute of Materials Science and Engineering, NETME Centre, Faculty of Mechanical Engineering, Brno University of Technology, Technická 2896/2, CZ-61669 Brno, Czech Republic*
[2]*Central European Institute of Technology, CEITEC MU, Masaryk University, Kamenice 753/5,CZ-625 00 Brno, Czech Republic*
[3]*Aalto University School of Engineering, Laboratory of Engineering Materials, PL 14200, FI-00076 Aalto, Finland*
[4]*Material Physics Laboratory, Lappeenranta University of Technology, Laitaatsillantie 3, FI-57170 Savonlinna, Finland*

Abstract. The effect of shear deformation on Ni_2MnGa magnetic shape memory alloy has been investigated using *ab initio* electronic structure calculations. We used the projector-augmented wave method for the calculations of total energies and stresses as functions of applied affine shear deformation. The studied nonmodulated martensite (NM) phase exhibits a tetragonally distorted $L2_1$ structure with $c/a > 1$. A large strain corresponding to simple shears in <100>{001}, <001>{100} and <010>{100} systems was applied to describe a full path between two equivalent NM lattices. We also studied <10-1>{101} shear which is related to twining of NM phase. Twin reorientation in this system is possible, because applied positive shear results in path with significantly smaller energetic barrier than for negative shear and for shears in other studied systems. When the full relaxation of lattice parameters is allowed, the barriers further strongly decrease and the structures along the twinning path can be considered as orthorhombic.

1 Introduction

Much attention has been paid to the Ni-Mn-Ga magnetic shape memory alloys because they exhibit interesting properties such as a giant magnetic field-induced strain (MFIS) of several percent [1]. This effect occurs in martensite phase, i.e. below the martensitic transformation temperature at which a high-temperature cubic phase, austenite, transforms to a phase with lower symmetry, martensite. The MFIS is a consequence of the coupling between the ferromagnetic microstructure and ferroelastic martensite microstructure, which results in a reorientation of martensite twins and the giant strain. Large magneto-crystalline anisotropy and high mobility of martensite twin boundaries are important factors enabling the MFIS [2–5]. From an atomistic point of view, the reorientation of twins is characterized by a diffusionless and completely reversible change of the crystal structure orientation from one martensite twin variant to another.

Several types of martensites have been observed in the Ni-Mn-Ga system. While near stoichiometric Ni_2MnGa shows cubic $L2_1$ symmetry in the austenitic phase, the structure of martensitic phase depending on temperature and exact composition are referred as (pseudo-)tetragonal or orthorhombic and can exhibit a modulation. The modulation means a shuffle of (110) planes of $L2_1$ structure in [1-10] direction with different periodicity [6]. Modulation with a periodicity of ten lattice planes (10M) or even fourteen lattice planes (14M) has been reported for structures with $c/a < 1$, which exhibits the MFIS of 6% [7,8] or 10%, respectively [9]. The third martensitic phase observed in Ni-Mn-Ga alloys has non-modulated (NM) tetragonal structure with $(c/a)_{NM} \approx 1.17–1.23$, which can be described as body-centered tetragonal unit cell $L1_0$ [10]. The MFIS reported in this phase is not larger than ~0.1% [11]. However, a MFIS of 12% has recently been reported in the special case of NM phase with reduced $(c/a)_{NM} = 1.147$, achieved by simultaneous doping by 4 at. % of Cu and Co [12]. In addition, a premartensite exists above the martensitic transformation temperature and exhibits cubic structure with symmetry reduced by modulation with periodicity of six lattice planes (6M) [13]. The assumed phase sequence starting from high temperatures is then $L2_1 \rightarrow 6M \rightarrow 10M \rightarrow 14M \rightarrow NM$ during cooling [14]. Moreover, a mixture of modulated with non-modulated martensite can be found coexisting in one sample for particular compositions [15].

The concept of adaptive martensite has been proposed on basis of work of Khachaturyan *et al.* [16] to describe 10M and 14M structures. It alternatively interprets the modulated martensites as a periodically nanotwinned tetragonal NM phase with a nanotwin period corresponding to the modulation period [17]. Thus the modulated structures can be described by an alternating sequence of nanotwins with a width of three (101) lattice planes in one orientation and width of two planes in the other for 10M [18] structure or by alternating nanotwins of width five and two (101) lattice planes for 14M structure [19,20]. The alternating nanotwins result in monoclinic symmetry of both structures, which are

[a] Corresponding author: zeleny@fme.vutbr.cz

Article available at http://www.matec-conferences.org or http://dx.doi.org/10.1051/matecconf/20153305006

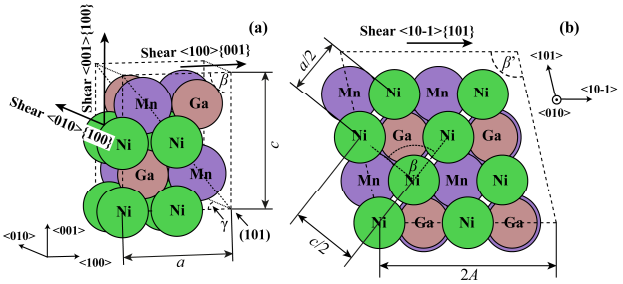

Figure 1. Simulation cells for <100>{001}, <001>{100}, <010>{100} shears (a) and <10-1>{101} twining shear (b). Directions of applied deformations, lattice parameters and lattice angles are shown. For <10-1>{101} twining shear the monoclinic lattice constant A and both angles are marked: "tetragonal" angle β and monoclinic angle β'. For better understanding the 2×1×2 cell is shown in this case instead of simulation cell with 8 atoms only.

denoted in literature as $(3\text{-}2)_2$ and $(5\text{-}2)_2$, respectively. This concept has been recently proved by DFT calculation with very precise settings. When the monoclinic variation of the simulated supercell is allowed, the $(5\text{-}2)_2$ nano-twinned structure exhibits almost the same total energy as NM structure and the energy of the $(3\text{-}2)_2$ nano-twinned structure is just slightly larger [21]. These energies are considerably lower than that of the modulated pseudo-tetragonal and premartensite structures. Such energy levels also correspond to the sequence of phase transformations with decreasing temperature.

Whereas the relative stability of different phases has been clarified, the detailed atomistic description of martensitic or intermartensitic transformations is still missing as well as the mechanism of twin reorientation, i.e. twin boundary motion. The mobility of twin boundaries has been described by the twinning stress, which is typically defined as the stress needed for twin boundary motion. Twin boundaries with low twinning stress (<1 MPa) are often referred to as highly mobile [22,23]. Different twinning modes can arise in the martensite such as as *a*–*c*, *a*–*b*, or *b*–*c* twinning, as well as monoclinic twinning [24,25] forming the hierarchical twin microstructure [26]. Only reorientation due to motion of the *a*–*c* twin boundaries is relevant for the MFIS [27]. In addition two types of *a*–*c* twin boundaries with different mobility have been observed in 10M martensite. Type I twin boundaries are exactly parallel to (101) plane, while Type II twin boundaries are approximately parallel to (10 1 10) using cubic coordinates, i.e. they are tilted 4° from (101) plane. [28,29]. The Type I exhibits strong decreasing dependency of the twinning stress with increasing temperature, whereas the twinning stress of Type II is nearly temperature independent and sufficiently low in a relatively wide temperature range [30,31]. The mechanism of reorientation in NM martensite is based on shear strain in <10-1>{101} system, thus the twinning stress is related to the shear stress in (101) plane and elastic shear modulus [32]. However, the motion of twin boundary is not so simple because the activation energy of the shear induced coherent motion process is not of the same order of magnitude as the magnetocrystalline anisotropy energy which was shown by quasistatic DFT simulations [33,34]. The mechanism includes also twinning dislocations slip along the twinning interfaces, which was confirmed by an experimental transmission electron microscopy measurement [35-37,17] and also by DFT calculations in combination with the Peierls–Nabarro model [32].

In this work, we present a detailed first-principle or *ab-initio* investigation of shear in different shear systems of Ni_2MnGa with NM crystal structure. It allows us to estimate the transformation path and energetic barrier between two equivalent NM lattices as well as the shear stress along the path and ideal shear strength.

2 Computational method

The quantum-mechanical framework of our *ab-initio* investigation is spin-density functional theory. The calculations were performed using the Vienna *ab-initio* simulation package (VASP) [38] in which the electron-ion interaction is described by projector-augmented wave (PAW) potentials [39,40]. The electronic orbitals were expanded in terms of plane waves with a maximum kinetic energy of 600 eV. We use the gradient-corrected exchange-correlation functional proposed by Perdew, Burke, and Ernzerhof [41]. The Brillouin zone (BZ) was sampled using a Γ-point centred mesh with the smallest allowed spacing between k-points equal to 0.1 $Å^{-1}$ in each direction of the reciprocal lattice vectors. This setting ensures constant k-points density in all our calculations. The integration over the BZ used the Methfessel-Paxton smearing method [42] with 0.02 eV smearing width. Settings for k-point density and smearing width have been obtained with help of adaptive smearing method [43]. The total energy was calculated with a high precision, converged to 10^{-7} eV per computational cell.

To describe the NM martensite we use the tetragonally distorted $L2_1$ cell with 16 atoms and equilibrium lattice parameters a = 5.3857 Å and $(c/a)_{NM}$ = 1.247 (see Fig. 1(a)). We investigate the response of the described unicell to affine shear deformation by applying shear strains in three different shear systems: <100>{001}, <001>{100} and <010>{100}. For <100>{001} system the affine shear deformation means that all atoms are shifted parallel to the direction of shearing [100] by a distance proportional to their perpendicular distance from the fixed basal plane (001). The affine shear deformation changes only the lattice vectors, while the fractional coordinates of the atomic positions within the cell remain unchanged [44]. Within this process the symmetry of the structure is reduced from tetragonal to monoclinic. As a measure of the shear deformation we have chosen the value of applied strain $\varepsilon_{100||001}$, which is calculated from the displacement Δx_{100} of the top plane (001) relative to the bottom plane (001) of the computational cell divided by their distance (lattice constant c). This ratio also corresponds to the tangent of the shear angle, which is equal to 90° – β monoclinic lattice angle. However, the tetragonal symmetry is renewed for some large strain, because at some point the

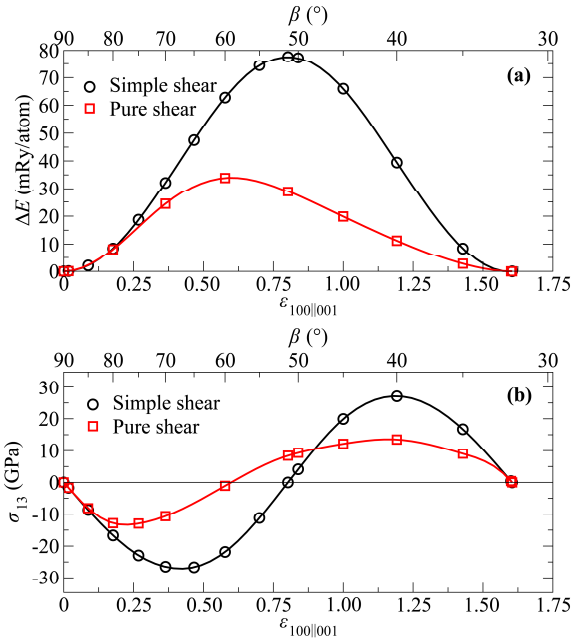

Figure 2. The energy-strain (a) and stress-strain (b) curves for shear in <100>{001} system. Corresponding values of lattice angle β are also shown on the x axis.

atoms will reach equivalent positions to the positions at the beginning. In other shear systems the process differs only in shifted planes and directions. A different monoclinic cell with 8 atoms has been used for simulation of shear in <10-1>{101} system which corresponds to shear related to twining of NM phase. In Fig. 1(b) the tetragonal symmetry corresponds to the cell with monoclinic angle equal to 102.52° and (101) plane of NM structure is (001) plane in the simulation cell.

A quasi-reversible deformation process at zero absolute temperature was assumed for all types of deformation. We considered two modes of shearing, as defined by Ogata *et al.* [45], pure and simple shear. Simple shear means that the shear deformation is not followed by a relaxation of the shape of the sheared cell and the positions of the atoms. Pure shear implies a full relaxation of the cell (shape, volume and atomic coordinates), with the only constraint that the shearing angle is fixed; i.e., all components of the stress tensor σ_{ij} except one (σ_{13} or σ_{12}) have to vanish after relaxation. However, the effect of atomic relaxation can be neglected due to their small contribution. Thus, only cell shape and volume relaxations were allowed in our simulations. The structural relaxation was performed using the external optimizer GADGET developed by Bučko *et al.* [46], which allows the use of symmetry-adapted generalized coordinates. Relaxation was stopped when all components of the stress tensor (except σ_{13} or σ_{12}) computed via the generalized virial theorem [47] were converged to within 0.1 GPa.

3 Results

We consider three inequivalent shear deformations in (001), (010) and (100) planes of Ni_2MnGa NM structure, namely <100>{001}, <001>{100} and <010>{100} shears. The simple shears acting in (001) basal plane are equivalent in both directions [100] and [010] parallel with this plane, thus the <100>{001} is equivalent with <010>{001}. The strain can be calculated as $\varepsilon_{100||001} = \tan(90° - \beta) = \Delta x_{100}/c$. Both simple shears acting in [001] direction are equivalent in planes (100) and (010), thus <001>{100} is equivalent with <001>{010} and $\varepsilon_{001||100} = \tan\beta = \Delta x_{001}/a$. Finally, the simple shear in <010>{100} system is equivalent with shear in <100>{010} system because in both cases the square basal plane of crystal structure is distorted. The strain $\varepsilon_{010||100} = \tan(90° - \gamma) = \Delta x_{010}/a$. This inequivalency of three shear systems is result of tetragonal symmetry of NM, because in cubic structure all six mentioned shears will exhibits same results. In this work another shear system <10-1>{101} is also studied. It corresponds to the twin reorientation, because both twin variants of NM structure can be found on this deformation path. Computational cell used for this path exhibits monoclinic angle $\beta' = 102.52°$, therefore applied strain is calculated as $\varepsilon_{10\text{-}1||101} = \tan(90° - \beta') - \tan 102.52°$. All energies are shown with respect to the energy equilibrium NM structure.

3.1. <100>{001} shear

The energy- and stress-strain curves for NM structure under <100>{001} shear are shown in Fig. 2. The full shear deformation path corresponds to the applied strain $\varepsilon_{100||001} = 1.604$, where body-centered tetragonal symmetry of NM is renewed, because atoms occupy the same positions as at the beginning. Structures along the path between the first and the last point exhibit monoclinic symmetry, with only one exception in the middle of the path at $\varepsilon_{100||001} = 0.802$ where symmetry is simple tetragonal with $c/a < 1$. At this point the metastable transition state (TS) with highest energy is reached, because the Ni atoms occupy the same position as in the origin, but Mn and Ga atoms are placed at the same x-coordinate as Ni atoms, which results in very short interatomic distances and simple tetragonal symmetry. The height of the energy barrier in TS is equal to 77.62 mRy/atom. This barrier decreases more than 50% to 28.88 mRy/atom for pure shear when relaxation of lattice parameters is allowed. The lattice relaxation also results in the shift of the position of TS to $\varepsilon_{100||001} = 0.555$. As can be seen in Fig. 2(a) the curve after relaxation is symmetric with respect to the angle β whereas the curve for simple shear was symmetric with respect to the applied strain.

The corresponding stress-strain curves in Fig. 2(b) show a stress response of the crystal on the applied strain. The maxima (or minima) on these curves correspond to the values of the theoretical or ideal shear strength (ISS) which is related to the stress necessary for the nucleation of a dislocation and for the formation of stacking faults in this shear system. The absolute value of ISS for simple shear is 26.6 GPa whereas for pure shear this value is 13.5 GPa. However, the ISS for simple shear is not very meaningful value because also other components of stress tensor are not equal to zero and can be even bigger than σ_{13} component. There is also a point in the middle of each

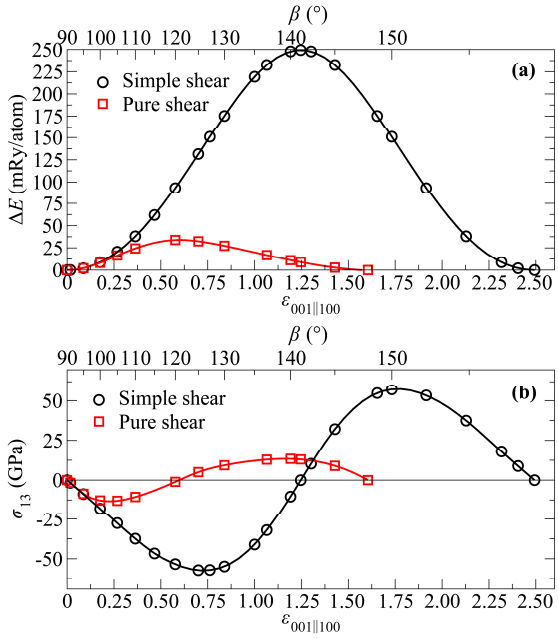

Figure 3. The energy-strain (a) and stress-strain (b) curves for shear in <001>{100} system. Corresponding values of lattice angle β are also shown on the x axis.

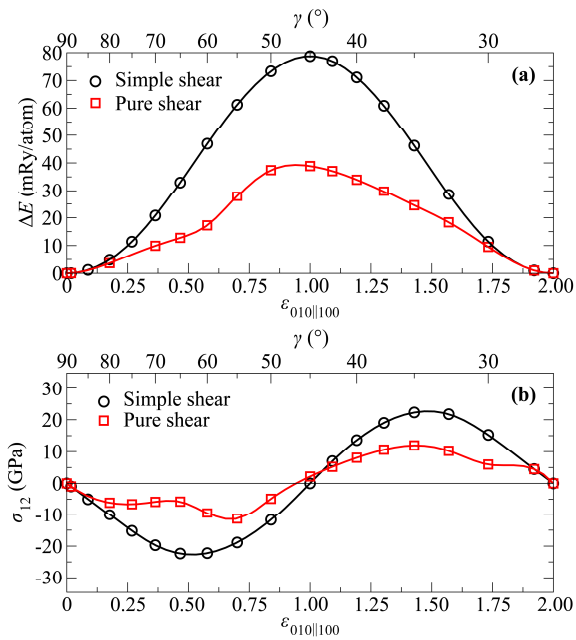

Figure 4. The energy-strain (a) and stress-strain (b) curves for shear in <010>{100} system. Corresponding values of lattice angle γ are also shown on the x axis.

path with $\sigma_{13} = 0$ which corresponds to the TS, because in this metastable state the structure is not under stress at all.

3.2 <001>{100} shear

The situation is different for <001>{100} system, because the shear is applied in [001] direction which corresponds to the longest lattice parameter c of the structure. Thus the large strain equal to $\varepsilon_{001||100} = 2.493$ has to be applied to obtain the same structure as in the origin. The TS at $\varepsilon_{001||100} = 1.247$ lies about 249.38 mRy/atom higher than the equilibrium structure (see Fig. 3(a)). This value is more than three times higher compare to <100>{001} shear because interatomic distances in the plane perpendicular to the shear plane are much shorter and larger lattice distortion is necessary to accommodate the stress. Of course the ISS for simple shear in this system is also much larger and equal to 57.2 GPa (see Fig. 3(b)). However, when the relaxation of the lattice parameters is allowed we obtain the same profile of energy- and stress-strain curves as in the case of <100>{001} pure shear. It happens because during relaxation process the lattice parameter a perpendicular to the shear plane is largely expanded and the lattice parameter c is contracted. After relaxation we can find exactly the same structures along the deformation path for <100>{001} shear and <001>{100} shear. When strain $\varepsilon_{001||100} = 1.604$ is applied the NM structure is again obtained but is rotated.

3.3 <010>{100} shear

In the <010>{100} shear the basal plane of the tetragonal lattice with square geometry is distorted, thus the structure equivalent to the origin is reached at $\varepsilon_{010||100} = 2$ and $\gamma = 26.57°$ (see Fig. 4). The TS for simple shear lies at $\varepsilon_{010||100} = 1$, where symmetry of the structure is simple tetragonal with $c/a > 1$. For pure shear the top of the barrier is just slightly shifted out of this position. The heights of the barriers are 78.7 mRy/atom and 38.9 mRy/atom for simple and pure shear, respectively. The ISS for simple shear is 22.4 GPa. The stress-strain curve for pure shear exhibits more extremes than for simple shear. However, the global minimum and maximum correspond almost to the same value of the ISS which is 12.0 GPa.

3.4 <10-1>{101} shear

The shear in three previously discussed shear systems does not depend on the sign of applied strain. Increasing or decreasing of the shear angle results in the same structures before and also after relaxation. This is not true for <10-1>{101} where the tetragonal NM structure corresponds to the monoclinic cell with angle $\beta' = 102.52°$, thus the structure after applying shear strain will depend on the shear sign. The negative strain increases the monoclinic angle and leads to the so called anti-twining shear, because structures along the path exhibit much higher energies than the NM structure and large strain has to be applied to reach tetragonal symmetry again. On the other hand, when the positive strain is applied the resulting energies are much lower and deformation path is much shorter which corresponds to the twining shear.

For anti-twining simple shear the original structure is again reached for $\varepsilon_{10\text{-}1||101} = -1.604$, however this structure corresponds to the opposite orientation of twin than in the origin. Because the path is symmetric with respect to the strain, the top of the barrier lies at $\varepsilon_{10\text{-}1||101} = -0.802$ and the height of the barrier is 70.5 mRy/atom (see Fig. 5(a)). The top of the barrier (34.0 mRy/atom) is shifted closer to the origin for the pure anti-twining shear and lies at $\varepsilon_{10\text{-}1||101} = -0.617$. The corresponding ISS is 25.8 GPa and

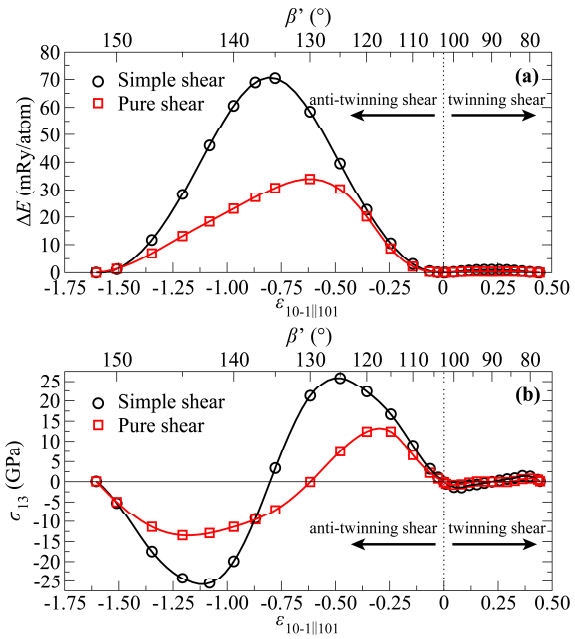

Figure 5. The energy-strain (a) and stress-strain (b) curves for twinning and anti-twinning shear in <10-1>{101} system. Corresponding values of lattice angle β are also shown on the x axis.

13.5 GPa for simple and pure shear, respectively (see Fig. 5(b)).

The detailed look on the twining shear is shown in Fig. 6. The opposite twin orientation is reached at $\varepsilon_{10\text{-}1||101} = 0.444$ and monoclinic angle $\beta' = 77.48$. The barrier is much smaller than in all the above discussed shear system even for simple shear. The height of the barrier is 1.04 mRy/atom only (see Fig. 6c). Because this path is symmetric with respect to strain as well as with respect to monoclinic angle, the top of the barrier can be found at $\varepsilon_{10\text{-}1||101} = 0.222$ which corresponds to $\beta' = 90°$. The ISS corresponding to simple twining shear is 1.46 GPa. When relaxation of atomic coordinates is allowed, the energy-strain curve has a different shape, because it exhibits a local minimum in the middle of the path and two maxima. Energies at these maxima are 0.394 mRy/atom. The highest absolute value of the stress along pure twining shear path is 0.80 GPa which corresponds to the ISS. The relaxation of lattice dimensions has also another effect. When a simple shear strain is applied and monoclinic angle β' decreases, the "tetragonal" angle β grows in the first half of the path up to 91.5° and then decreases back to 90° (see Fig. 6c). So, the symmetry is only monoclinic along simple shear path. For pure shear the "tetragonal" angle β is near to 90° and structures after relaxation along the whole path can be considered as orthorhombic. Thus, the relaxation increases the symmetry of these structures.

4 Conclusions

The shear in four inequivalent systems of Ni_2MnGa NM structure has been studied using the PAW *ab-initio* method. The deformation paths for <100>{001} simple shear and <010>{100} simple shear exhibit the height of the barrier approximately 80 mRy/atom. Just slightly smaller barrier has been found for anti-twining deformation path in <10-1>{101}. These barriers decrease approximately about 50% for pure shear where relaxation of lattice parameters was allowed. Similar 50% decreasing was observed also for ideal shear strength approximately from 26 GPa to 13GPa. The barrier for simple shear in <001>{100} system is much higher and equal to 250 mRy/atom due to the shorter interlayer distances between shear planes {100}. Analogically, also the ideal shear strength is much higher and equal to 57 GPa. On the other hand, the path for pure shear is identical with the path for pure shear in <100>{001} system due to relaxation of lattice parameters.

Compared to above mentioned cases the twining path in the <10-1>{101} system exhibits significantly smaller energy barrier equal to 1 mRy/atom, which further decreases after relaxation to 0.4 mRy/atom. Additionally, the structures after relaxation exhibit orthorhombic symmetry along whole twinning deformation path. The highest value of stress for pure shear corresponds to 0.8 GPa, which is in the same order of magnitude as the theoretical values reported for other shape memory materials [48]. These small values for shear stress and energy barrier shows that the twin reorientation can be realized in <10-1>{101} shear system and by the path with orthogonal crystal lattices. Let us note that the presented values of energies and stresses along the twining path are not exact values for twin reorientation because calculated energy barrier is still about one order bigger than previously published energies of magnetic anisotropy in NM phase and stresses along described path are bigger than reported values for twining stress. However, both quantities can be further decreased by presence of dislocations in the shear plane (101) or by increasing temperature.

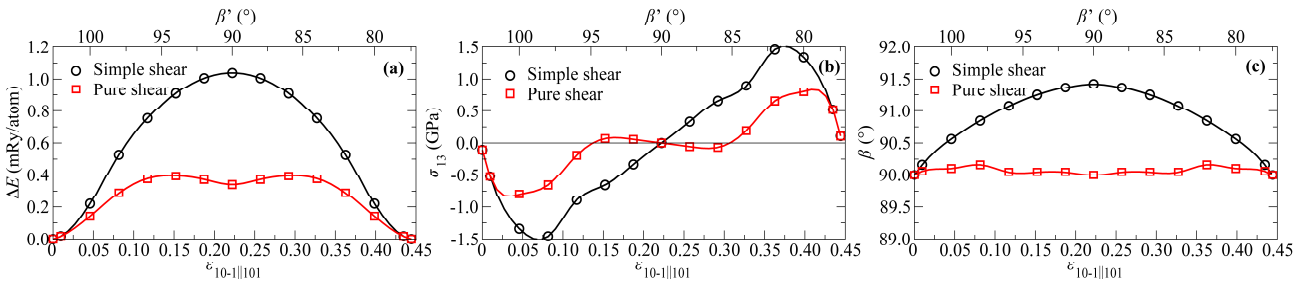

Figure 6. The detail of energy-strain curve (a), stress-strain curve (b) and "tetragonal" angle β as a function of strain (c) for twinning shear in <10-1>{101} system. Corresponding values of monoclinic angle β' are also shown on the x axis.

Acknowledgements

This research has been supported by the Ministry of Education, Youth and Sports within the support programme „National Sustainability Programme I“ (Project NETME CENTRE PLUS – LO1202), by the Grant Agency of the Czech Republic (Projects No. 14-22490S and No. 13-35890S). The access to the CERIT-SC computing and storage facilities provided under the programme Center CERIT Scientific Cloud, part of the Operational Program Research and Development for Innovations, Reg. No. CZ. 1.05/3.2.00/08.0144, is greatly appreciated.

References

1. K. Ullakko, J. K. Huang, C. Kantner, R. C. O'Handley, V. V. Kokorin, Appl. Phys. Lett. **69**, 1966 (1996)
2. M. E. Gruner, P. Entel, I. Opahle and M. Richter, J. Mater. Sci. **43**, 3825 (2008)
3. O. Söderberg, Y. Ge, A. Sozinov, S.-P. Hannula, and V. K. Lindroos, in *Handbook of Mag. Mat.*, edited by K. H. J. Buschow, Vol. 16, pp. 1–39 (Elsevier, Amsterdam, 2006)
4. O. Heczko, N. Scheerbaum, and O. Gutfleisch, in *Nanoscale Magnetic Materials and Applications*, edited by J. Liu, E. Fullerton, O. Gutfleisch, and D. Sellmyer, pp. 339–439 (Springer, Berlin, 2009)
5. M. Acet, L. Mañosa, and A. Planes, in *Handbook of Mag. Mat.*, edited by K. H. J. Buschow, Vol. 19, pp. 231–289 (Elsevier, Amsterdam, 2011)
6. K. Otsuka, T. Ohba, M. Tokonami, and C. M. Wayman, Scr. Metall. Mater. **29**, 1359 (1993)
7. S. J. Murray *et al*., Appl. Phys. Lett. **77**, 886 (2000)
8. O. Heczko, A. Sozinov, and K. Ullakko, IEEE Trans. Magn. **36**, 3266 (2000)
9. A. Sozinov, A. A. Likhachev, N. Lanska, and K. Ullakko, Appl. Phys. Lett. **80**, 1746 (2002)
10. N. Lanska, O. Söderberg, A. Sozinov, Y. Ge, K. Ullakko, and V. K. Lindroos, J. Appl. Phys. **95**, 8074 (2004)
11. V. A. Chernenko, M. Chmielus and P. Müllner, Appl. Phys. Lett. 95, 104103 (2009)
12. A. Sozinov, N. Lanska, A. Soroka, and W. Zou, Appl. Phys. Lett. **102**, 021902 (2013)
13. C. P. Opeil *et al.*, Phys. Rev. Lett. **100**, 165703 (2008)
14. V. A. Chernenko, C. Segui, E. Cesari, J. Pons, V. V. Kokorin, Phys. Rev. B **57**, 2659 (1998)
15. A. Çakr, L. Righi, F. Albertini, M. Acet, M. Farle, and S. Aktürk, J. Appl. Phys. **114**, 183912 (2013)
16. A. G. Khachaturyan, S. M. Shapiro, and S. Semenovskaya, Phys. Rev. B **43**, 10832 (1991)
17. Y. Ge, N. Zárubová, O. Heczko and S.-P. Hannula, Acta Mater. **90**, 151 (2015)
18. S. Kaufmann *et al.*, New J. Phys. **13**, 053029 (2011)
19. J. Pons,V. A. Chernenko, R. Santamarta, and E. Cesari, Acta Mater. **48**, 3027 (2000)
20. S. Kaufmann, U. K. Rößler, O. Heczko, M. Wuttig, J. Buschbeck, L. Schultz, and S. Fähler, Phys. Rev. Lett. **104**, 145702 (2010)
21. M. E. Gruner, S. Fähler, and P. Entel, Phys. Status Solidi B **251**, 2067 (2014)
22. A. Sozinov, A. A. Likhachev, N. Lanska, O. Söderberg, K. Ullakko, V. K. Lindroos, Mater. Sci. Eng., A **378**, 339 (2004)
23. L. Straka, O. Heczko, H. Hänninen, Acta. Mater. **56**, 5492 (2008)
24. K. Bhattacharya, *Microstructure of Martensite: Why It Forms and How It Gives Rise to the Shape-Memory Effect* (OUP, Oxford, 2003)
25. O. Heczko, L. Straka, H. Seiner, Acta Mater. **61**, 622 (2013)
26. H. Seiner, L. Straka, O. Heczko, J. Mech. Phys. Solids **64**, 198 (2014)
27. O. Heczko, Mater. Sci. Technol. **30**, 1559 (2014)
28. A. Sozinov, N. Lanska, A. Soroka, L. Straka, Appl. Phys. Lett. **99**, 124103 (2011)
29. L. Straka, O. Heczko, H. Seiner, N. Lanska, J. Drahokoupil, A. Soroka, S. Fähler, H. Hänninen, A. Sozinov, Acta Mater. **59**, 7450 (2011)
30. L. Straka, A. Soroka, H. Seiner, H. Hänninen, and A. Sozinov, Scripta Mater. **67**, 25 (2012)
31. M. Veis, L. Beran, M. Zahradnik, R. Antos, L. Straka, J. Kopecek, L. Fekete, and O. Heczko, J. Appl. Phys. **115**, 17A936 (2014)
32. J. Wang and H. Sehitoglu, Acta Mater. **61**, 6790 (2013)
33. M. E. Gruner, P. Entel, I. Opahle, and M. Richter, J. Mater. Sci. **43**, 3825 (2008)
34. M. E. Gruner and P. Entel, J. Phys.: Condens. Matter **21**, 293201 (2009)
35. Y. Ge, N. Zárubová, Z. Dlabáček, I. Aaltio, O. Söderberg, S.-P. Hannula (Eds.), *ESOMAT 2009–8th* (EDP Sciences, 2009)
36. N. Zárubová, Y. Ge, J. Gemperlová, A. Gemperle, S.-P. Hannula, Funct. Mater. Lett. **5**, 1250006 (2012)
37. N. Zárubová, Y. Ge, O. Heczko, S.-P. Hannula, Acta Mater. **61**, 5290 (2013)
38. G. Kresse and J. Furthmüller, Phys. Rev. B **54**, 11169 (1996); Comput. Mater. Sci. **6**, 15 (1996)
39. P. E. Blöchl, Phys. Rev. B **50**, 17953 (1994)
40. G. Kresse and D. Joubert, Phys. Rev. B **59**, 1758 (1999)
41. J. P. Perdew, K. Burke, and M. Ernzerhof, Phys. Rev. Lett. **77**, 3865 (1996); **78**, 1396(E) (1997)
42. M. Methfessel and A. T. Paxton, Phys. Rev. B **40**, 3616 (1989)
43. T. Björkman and O. Grånäs, J. Quantum Chem. **111**, 1025 (2011)
44. M. Jahnátek, J. Hafner, and M. Krajčí, Phys. Rev. B **79**, 224103 (2009)
45. S. Ogata, J. Li, and S. Yip, Science **298**, 807 (2002)
46. T. Bučko, J. Hafner, and J. G. Ángyán, J. Chem. Phys. **122**, 124508 (2005)
47. O. H. Nielsen and R. M. Martin, Phys. Rev. Lett. **50**, 697 (1983); Phys. Rev. B **32**, 3780 (1985)
48. S. Kuramotoa, N. Nagasakoa, T. Furutaa, Z. Horita, J. Alloys Compd. **577S**, S147 (2013)